

Improved OpenCL-based Implementation of Social Field Pedestrian Model

Bin Yu ^{*} Ke Zhu [†] Kaiteng Wu [‡] Michael Zhang [§]

Abstract

Two aspects of improvements are proposed for the OpenCL-based implementation of the social field pedestrian model. In the aspect of algorithm, a method based on the idea of divide-and-conquer is devised in order to overcome the problem of global memory depletion when fields are of a larger size. This is of importance for the study of finer pedestrian walking behavior, which usually requires larger fields. In the aspect of computation, the OpenCL heterogeneous framework is thoroughly studied. Factors that may affect the numerical efficiency are evaluated, with regarding to the social field model previously proposed. This includes usage of local memory, deliberate patch of data structures for avoidance of bank conflicts, and so on. Numerical experiments disclose that the numerical efficiency is brought to an even higher level. Compared to the CPU model and the previous GPU model, the current GPU model can be at most 71.56 and 13.3 times faster respectively so that it is more qualified to be a core engine for analysis of super-large scale crowd.

Keywords: Algorithm, Heterogeneous Parallel Computing, OpenCL, Pedestrian Flow

1 Literature Review

Since NVIDIA first proposed the term “Graphics Processing Unit”, known as GPU, in the year of 1999, GPU has grown into a heterogeneous parallel computing architecture, which is often used to solve complicated scientific and engineering problems. The two most commonly used platforms are OpenCL and CUDA. Scholars from different disciplines reported successful applications of the two, like [1, 2] in mathematics, [3] in physics, [4–7] in computer science, [8–11] in seismic engineering, [12, 13] in bioinformatics, [14] in communication, [15–18] in image processing, and so on.

A crowd is fundamentally a many-body system that would require quite a lot of computation efforts for analysis. GPU should naturally provide a good

^{*}Corresponding author, Tongji University, P.R.C., by@tongji.edu.cn

[†]Tongji University, P.R.C., 1213235421@qq.com

[‡]Tongji University, P.R.C., kaitengwu@163.com

[§]University of California at Davis, U.S.A., hmzhang@ucdavis.edu

solution to the problem in terms of numerical computation. Unfortunately, the research on GPU in the field of crowd simulation is far behind other disciplines. Before the authors, only a few scholars have been engaged in relevant research [19–22]. Furthermore, as far as the final results are concerned, their research findings are not exciting and suggest a space for further improvement. As referred by Molero *et al.* [10], developing a scalable and portable GPU parallel model is a challenge. Especially, in order to fully utilize the power of GPU, owing a suitable architecture is the key. In other words, for a math model, it can be well mapped into GPU only when its logic architecture is appropriate. With realizing the point, the authors decided to propose a field-based pedestrian model first after consideration [23]. In addition to the better modeling of crowd dynamics, the proposed continuous model has the advantage of easy discretization so that a discrete version and a later OpenCL-based implementation were developed. Yu *et al.* [24] reported that this can bring an at most 30.8 times speedup with comparison to the CPU model.

The paper is the follow-up research and tries to improve the work of [24] in two aspects. Firstly, it develops a method based on the idea of divide-and-conquer to solve the problem of global memory depletion when fields have a large geometric size. This is key as now it is possible to analyze super-large scale crowd’s finer walking behavior. Secondly, potential factors affecting OpenCL are thoroughly considered in order to further improve the numerical efficiency. The left content is organized as the following. A brief of the continuous and discrete social field pedestrian models is presented at first. The discussion of introduced improvements comes next. Then conducted numerical experiments are exhibited. The conclusion is given in the end.

2 Continuous and Discrete Models

Firstly, in order to avoid unnecessary confusion with the cellular automata, the term of space unit abbreviated as su is used to express the minimal discrete space. To save space, only a brief is given. Interested readers can refer to [23,24] for a detailed description of the models.

In the continuous model, a pedestrian’s physical movement is simulated as a response to the pedestrian’s subjective perception of the objective environment. The objective environment is represented by force incurred by presumed fields. To model various practical phenomena, total five kinds of fields are introduced, among which omnidirectional attractive and repulsive fields are to model influence of static openings and obstacles. Directional attractive and repulsive fields and recurrent repulsive fields are all to model influence due to neighboring pedestrians’ movement. But their evolution laws are different as they are targeting at walking behavior observed under different density regimes. Another point worthy of mention is introduction of the concept of regulation function. Through regulation functions, the objective environment around a pedestrian p represented by force can be adjusted correspondingly to form the dynamic subjective or perceived environment that is used to determine p ’s next movement.

In this way, pedestrians' intelligence can be well considered. Additionally it is stressed that the *local* density instead of the well-known macroscopic one should be used to reflect pedestrians' biased perception of the environment.

Except allowing the continuous model to own a larger degree of freedom, using the concept of field also leads to a straightforward discretization. As shown in the work of [24], a discrete model was derived. Especially, the concept of walk period was introduced. Using the concept, the variance of walking velocities of pedestrians can be well studied under the assumption that pedestrians' maximal speed is 1 su per tick. It should be noted that, for the discrete model, the assumption $v_{max} = 1$ is not insignificant, but one of the key points. More importantly, the method will not add additional complexities to the underlying logic, but it should be emphasized that the concept is related with some form of space fineness. Therefore, in the discrete model, pedestrians are allowed to occupy more than one su and the behavior of jostling can be studied. In the meantime, to ensure that, for a pedestrian p , one and only one su will be p 's center, it is ruled that p 's width and height can be different but must be odd su(s) like 1, 3, 5, ..., and so on.

3 Algorithm Related Improvement

3.1 Architecture of OpenCL-based Computation Model

Algorithm 1 OpenCL-based GPU Model

```

procedure MAIN
   $p \leftarrow$  simulation period
   $t \leftarrow 0$ 
  while  $t < p$  do
     $k$ -1. initialize the temporary storage;
     $k$ -2. determine pedestrians' next movement;
     $k$ -3. vote which pedestrian should occupy unoccupied su(s);
     $k$ -4. perform pedestrians' next movement;
     $k$ -5. write cached changes back;
   $t \leftarrow t + 1$ 

```

Algorithm 1 lists the architecture of the OpenCL-based model previously developed. As indicated, five sub-jobs will be repeated orderly at every simulation tick. In k -1, for each su, a work-item will be assigned to initialize the temporary storage allocated in the global memory space. In k -2, for each pedestrian, a work-item will be assigned to determine the pedestrian's next movement. In k -3, for each su, a work-item will be assigned to vote which pedestrian among the candidates should occupy if the su is unoccupied. In k -4, for each pedestrian, a work-item will be assigned. If the pedestrian's next movement is not still, the assigned work-item then checks whether the pedestrian is the one to occupy for the su(s) to be occupied. If yes, the pedestrian will be physically moved and

relevant changes will be buffered. Finally, in $k-5$, for each `su`, a work-item will be assigned to write the changes buffered in $k-4$ back to the global storage, which is camouflaged as a 3-D image.

When the discrete model was mapped into the OpenCL heterogeneous computing framework, mechanisms were introduced, among which two used to avoid atomic functions like `atomic_add` etc are worthy of little words. In real applications, using atomic functions is the direct way for solving competition among work-items. On the other hand, it should be noted that atomic functions would significantly harm the computation performance, especially when a global memory is being manipulated. Thus, to achieve a better performance, people will struggle to avoid atomic functions, if possible, even though this may generally require an overhaul. For our problem, competition could occur in the following two situations.

- s-1.** Fields stored in the shared 3-D image are updated due to pedestrians' movement.

Competition is solved through the concept of strength fan-out. It is observed that, for one memory storage place in the shared 3-D image, once a field's discrete geometry space is determined, the set of `sus` can be computed beforehand so that the memory storage place's content will be affected only if the field's central `su` belongs to the computed set. Furthermore, although the set of `sus` computed would change if the field is moving, the number of `sus` keeps unchanged so that the concept of strength fan-out is introduced. This can be illustrated by examining a recurrent repulsive field that is locating at the origin and whose discrete geometry space is 7×7 `sus`. Figures 1 and 2 give the discrete field strength incurred. According to figure 1, it is found that the presumed recurrent repulsive field's strength fan-out is 6 and the set of computed `sus` contains $(-1, -1)$, $(-1, 0)$, $(0, 0)$, $(1, 0)$, $(0, 1)$, and $(1, 1)$. Figure 3 demonstrates that, if the field's central `su` belongs to the computed set, the sect index of incurred discrete strength at the `su` $(2, 2)$ is always 1, meaning that the same global memory address will be accessed.

With the concept of strength fan-out, a big enough global memory space can be allocated beforehand to buffer field strength related changes made in $k-4$, which will be written back to the shared 3-D image all at once in $k-5$. In this way, no atomic function is required.

- s-2.** Pedestrians compete with each other for empty `su(s)`.

Competition is solved by the observation that at most 8 pedestrians will participate the occupancy competition of one `su` under the assumption $v_{max} = 1$. A register-vote mechanism is adopted. An enrollment container that can hold at most 8 pedestrians will be allocated for each `su`. For an empty `su`, pedestrians trying to occupy the `su` should register first at the `su`'s enrollment container ($k-2$). Later, an election among the registered pedestrians will be hold to determine who should occupy the `su` ($k-3$).

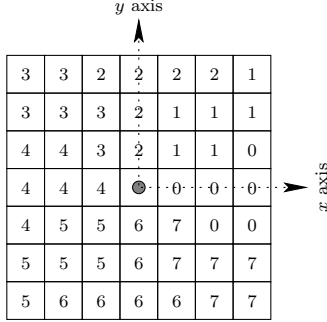


FIG. 1: This exhibits sect indexes of field strength incurred by the presumed recurrent repulsive field with $k = 1$ and $\alpha = -0.5$. A same sect index means that the same memory storage place is to be changed.

0.58	0.58	0.58	0.58	0.58	0.58	0.58
0.58	0.71	0.71	0.71	0.71	0.71	0.58
0.58	0.71	1.00	1.00	1.00	0.71	0.58
0.58	0.71	1.00	●	1.00	0.71	0.58
0.58	0.71	1.00	1.00	1.00	0.71	0.58
0.58	0.71	0.71	0.71	0.71	0.71	0.58
0.58	0.58	0.58	0.58	0.58	0.58	0.58

FIG. 2: This exhibits scalar values of field strength incurred by the presumed recurrent repulsive field.

3.2 Technical Problems Suffered

The foregoing methods both follow the same idea of preventing competition in expense of memory space, but a big difference does exist. For the method used to solve competition occurring in **s-2**, an upper-bound limit with regarding the required memory space exists since at most 8 pedestrians will compete with each other for occupancy of a su. Unfortunately, this is no more valid for the method used to solve competition occurring in **s-1**. When a field's discrete geometry space becomes larger, the corresponding strength fan-out increases. So is the required memory space. Table I lists strength fan-outs when different geometries are assumed for the presumed recurrent repulsive field.

In general, a field's discrete geometry will take a value shown in table I, thus is not large, but situations where a large geometry is used do exist. Firstly, a study of pedestrians' finer walking behaviors generally requires larger fields so

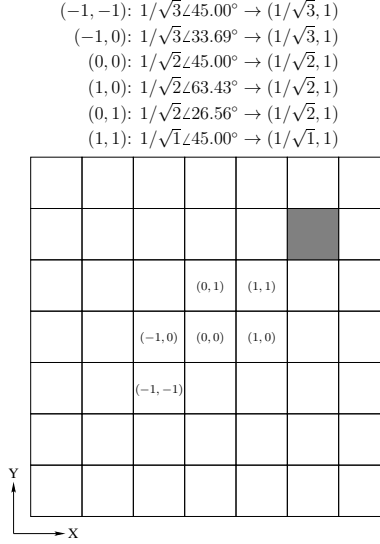


FIG. 3: This exhibits, for the presumed recurrent repulsive field, 6 sus exist so that, if the field's central su is one of them, the field can incur discrete strength at the su (2, 2) with the sect index value being 1.

that distant effect can be well considered. Secondly, pedestrians are allowed to occupy more than one su so that fields should be scaled up correspondingly. For the presumed recurrent repulsive field, table II lists the strength fan-outs for different geometries. As shown in figure 4, the strength fan-out is increasing at a dramatic rate.

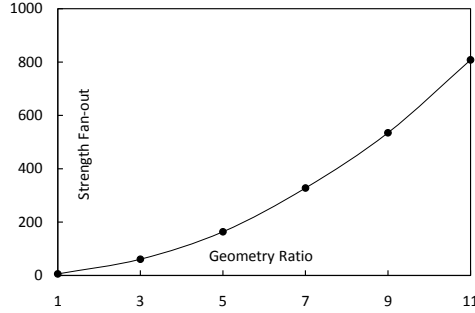


FIG. 4: Geometry Ratio vs. Strength Fan-out

The OpenCL-based implementation was developed for simulation of super-large scale crowd. Let us examine the memory space required to solve competition occurring in **s-1** if a half million population is simulated. To keep the discussion simple, the following assumptions are made. The whole discrete space

TABLE I: List of strength fan-outs

$wd \backslash ht$	1	3	5	7	9	11	...
1	0	1	2	3	4	5	
3	1	1	2	5	8	11	
5	2	3	4	6	10	14	\vdots
7	3	6	6	6	10	14	\vdots
9	4	8	9	10	11	15	
11	5	11	14	15	15	15	
\vdots				...			\ddots

TABLE II: This exhibits strength fan-outs when different geometries are assumed for the presumed recurrent repulsive field. For a ratio, the corresponding geometry's width and height will both equal to $7 * ratio$.

ratio	1	3	5	7	9	11
<i>strength fan-out</i>	6	61	164	328	535	808
m_{recur} ; byte	192	1952	5248	10496	17120	25856
M ; GB	0.7	7.3	19.6	39.1	63.8	96.3

is 1000×1000 and pedestrians are all of a geometry 1×1 su. Thus a half million population would actually mean that the macroscopic density is 0.5. All fields' geometry is same, so is their strength fan-out denoted as SF . For each su, the memory space m_{recur} required to store recurrent repulsive fields is then $SF * 8 * 4$ and the total memory space needed is $m = m_{attra} + m_{repul} + 2 * m_{recur}$. Lastly, multiplying m by the number of sus gives the total memory space M needed. Table II also lists values of m_{recur} and M . As shown, when fields' geometry is 21×21 , M already reaches to about 7.3 GB, not to say even larger sizes.

3.3 Solution Illustration

The former methodology is to cache all of the changes at a time and algorithm 2 lists the pseudo-code for recurrent repulsive fields. For directional attractive and repulsive fields, the algorithms are almost same. However this may cause the foregoing memory depletion problem.

$$\sum_{i=0}^{n-1} a[i] \stackrel{n=K*m}{=} \sum_{j=0}^{K-1} \sum_{i=0}^{m-1} a[j * K + i] \quad (1)$$

The proposed solution is based on the observation that what is really cared is the final change summed up. The summation way is of less importance. As the aforementioned one-step summation may cause the problem of memory depletion, the multi-step summation can be used instead. This is mathematically

Algorithm 2 One-Step Sum For Recurrent Repulsive Fields

```
1: procedure ONE-STEP SUM IN  $k-4$  (float cache[])
2:   for all  $c \in \text{sus}$  do
3:     float  $*s \leftarrow \text{FINDCACHE}(\text{cache}, c)$ 
4:      $\text{COMPUTEANDCACHECHANGES}(s)$ 

5: procedure ONE-TIME SUM IN  $k-5$  (float cache[])
6:   for all  $c \in \text{sus}$  do
7:     float  $*s \leftarrow \text{FINDCACHE}(\text{cache}, c)$ 
8:      $\text{sum} \leftarrow 0$ 
9:     for  $i = 0$  to  $8 * \text{strength fan-out} - 1$  do
10:       $\text{sum} \leftarrow \text{sum} + s[i]$ 
11:      $\text{WRITEBACK}(c, \text{sum})$ 
```

equivalent to Eq. 1. When n is too large, it is fine to divide it into the multiplication of two numbers, i.e. $n = K * m$. Especially, with keeping one number constant, an upper bound of memory consumption can be set up.

Algorithm 3 Multi-Step Sum For Recurrent Repulsive Fields

```
1: procedure MULTI-STEP SUM IN  $k-4$  (float cache[])
2:   for all  $c \in \text{sus}$  do
3:     float  $s[K] \leftarrow \text{FINDCACHE}(\text{cache}, c)$ 
4:      $m \leftarrow 8 * \text{strength fan-out} / K$ 
5:     for  $i = 0$  to  $m - 1$  do
6:        $\text{COMPUTEANDCACHESTEPCHANGES}(s, i)$ 

7: procedure MULTI-STEP SUM IN  $k-5$  (float cache[])
8:   for all  $c \in \text{sus}$  do
9:     float  $s[K] \leftarrow \text{FINDCACHE}(\text{cache}, c)$ 
10:     $\text{sum} \leftarrow 0$ 
11:    for  $i = 0$  to  $K - 1$  do
12:       $\text{sum} \leftarrow \text{sum} + s[i]$ 
13:     $\text{WRITEBACK}(c, \text{sum})$ 
```

The proposed methodology's pseudo-code is given in algorithm 3. With comparison to the one shown in algorithm 2, one additional loop between lines 5 and 6 is first noticed, which actually performs the inner summation of Eq. 1. More importantly, through the additional loop, the loop count of the one between lines 11 and 12 is bound to K . Correspondingly, this would limit the memory space required, i.e. **float**[K] in lines 3 and 9. In the up-to-date implementation, K is allowed to be 2, 4, 8, and 16 in order to use the built-in geometric function - *dot* product. Sometimes K may not divide n , i.e. $K \nmid n$. To solve, n can be extended to a multiplier of K by appending corresponding zero strength.

4 Computation Related Improvement

4.1 Structure of OpenCL

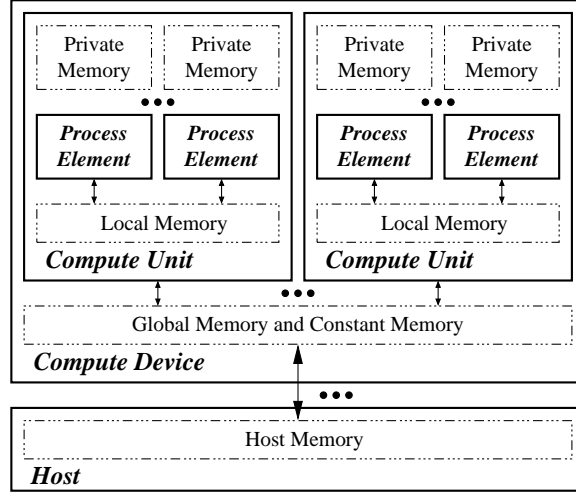


FIG. 5: OpenCL Architecture

Computation techniques are developed with the OpenCL architecture being kept in mind. Therefore it is worthy to briefly illustrate the architecture at first, as shown in figure 5. At the hardware level, an OpenCL computing environment is composed of a host and one or more compute devices. A compute device is composed of multiple compute units, each of which is further composed of multiple process elements. In the level of execution, compute unit and process element are also named work-group and work-item respectively. To work with OpenCL, the general work flow chart is as follows. Firstly, computation tasks to be fulfilled are programmed as kernels, using the OpenCL C dialect. Secondly, tasks are submitted to the command queue. The OpenCL computing environment then takes the full control of submitted tasks. For example, at a suitable time, it will pick an apt task and execute with appropriate global and local work sizes. In order to improve the numerical efficiency, OpenCL provides both task and data level of parallelism. The task level of parallelism is embodied by the fact that more than one task can be executed concurrently as multiple compute units exist. OpenCL provides the SIMD processing fashion for the data level of parallelism, which can be viewed in two sub-levels. Logically, when a task is executed, the kernel representing the task will be run literally at the same time by work-items distributed among more than one work-group. Therefore a work-group is a bunching of work-items, but not the most basic one, which is instead *warp* (Note: AMD calls this *wavefront*.) A warp is the smallest execution unit of code so that the same machine instruction will be emitted to all of

work-items in it. In this sense, the mechanism of warp provides the physical level of data parallelism.

In addition, the OpenCL memory model is noteworthy too, which is also exhibited in figure 5. Firstly, data stored in the host memory can not be directly accessed by compute devices and must be transferred to the global memory beforehand through relevant OpenCL functions. The global memory and constant memory can be accessed by all process elements in the same compute device. In addition, each compute unit has its own local memory that is accessible to all process elements in it. Lastly, each process element has the private memory, which can be accessed only by the process element itself. Except access privileges, the memory spaces are distinguished in aspects of band width, capacity, and so on. In terms of capacity, the global memory is largest and reaches to the level of gibibyte. Next is the local memory, which is generally in the level of kilobyte. The private memory is least that is generally 1 kilobyte or less. On the other hand, in terms of band width, the private memory is largest, then is the local memory. And the global memory is least.

4.2 Computational Techniques

With OpenCL’s architecture being thoroughly investigated, the following aspects are considered to improve the numerical efficiency.

Data Bandwidth In the former implementation, all computation work is fulfilled by directly manipulating data in the global memory after the transferring from the host memory. However this way does not fully consider the OpenCL memory model’s structure. In OpenCL devices, the local memory is on-chip and close to the process elements, thus is much faster than the global memory. By saying that, a more appropriate way to work with the memory model is as follows. Firstly, data is transferred from the host memory to the global memory. Secondly, for each work-group, the portion of data to be worked by the work-group is copied to the local memory through asynchronous copying functions like `async_work_group_copy` etc. Once computation work is done, data may be transferred back to synchronize the one stored in the host memory, if necessary.

Concurrency Formerly it is programmed so that tasks are almost executed in the order of submission. In addition, there is a strict execution sequence between CPU and GPU so that CPU has to wait GPU to finish all of the submitted tasks before starting to process routine work. Now the whole framework is re-organized so that 1. many times, more than one task can be executed simultaneously; 2. the strict sequence between CPU and GPU is weakened to a large extent and even disappears in some cases. Figure 6 exhibits the flow chart of jobs submitted. Further, to see in which time frame each submitted job is executed, a time profiling is fulfilled to one of numerical experiments conducted, as shown in figure 7.

Bank Conflict The way of emitting one machine instruction to all work-items bundled in the same warp at a time improves the degree of parallelism, but also

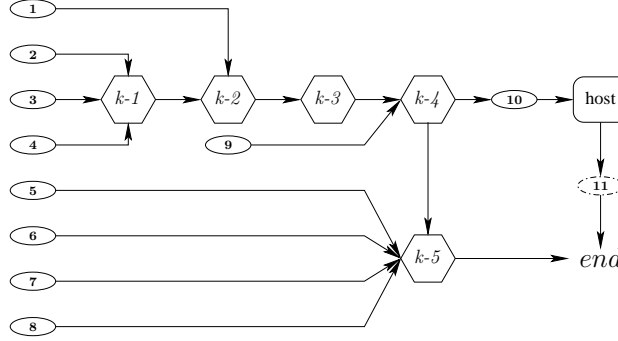


FIG. 6: This exhibits the flow chart of jobs that will be fulfilled by GPU and CPU at each simulation tick. Arabic numbers represent various buffer reading and writing tasks to be submitted to the OpenCL command queue. $k-1$, $k-2$, ..., $k-5$ are the kernels appearing in algorithm 1. After task no.10, the host, i.e. CPU, will start to process routine work. Especially, if occupancy state of openings is changed due to pedestrians' leaving and entering, additional tasks, i.e. task no.11, will be submitted correspondingly.

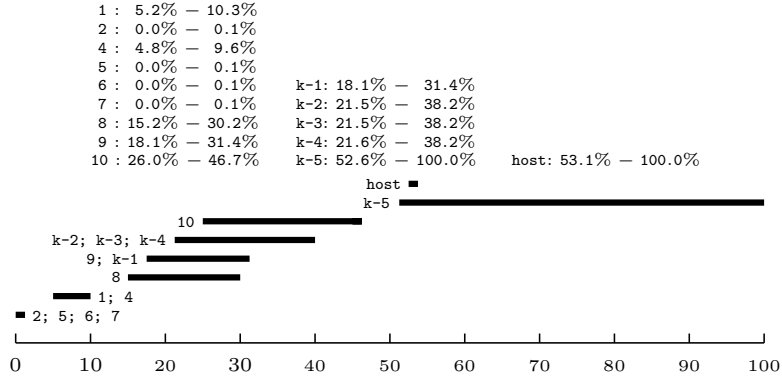


FIG. 7: This exhibits each job's time frame of execution in percentage. The ones for jobs no.3 and no.11 shown in figure 6 are missing due to usage of the periodic boundary condition. This also causes the time frame used by the host to be very short, which otherwise will largely overlap the one for job $k-5$ in reality. In addition, the shown ending time is the one when the installed event callback procedure is called, not exactly the one when the job is accomplished. This is why multiple jobs appear to end at the same time.

brings problems and difficulties deserving of attention. One is the so called bank conflict. In general, addresses of the local memory are grouped into banks. For work-items in the same warp, access of the local memory has to be serialized if the same bank is used. Thus, to avoid bank conflicts, a feasible way is post-

TABLE III: This summarizes severity and implementation difficulty of considered computational techniques. A smaller value means more severe or harder.

	Severity	Hardness
<i>Data Bandwidth</i>	①	⑥
<i>Competence</i>	②	①
<i>Divergence</i>	③	②
<i>Bank Conflict</i>	④	④
<i>Concurrency</i>	⑤	⑤
<i>Locality of Access</i>	⑥	③

patch. For example, in the current implementation, internal `C structs` used by work-items will be intentionally patched to a size of a prime integer by appending a corresponding number of bytes. In this way, bank conflicts can be prevented at most.

Divergence Another serious problem caused by the SIMD processing fashion is divergence. As all work-items in a warp will execute the same machine instruction at a time, existence of branch statements such as `if-else`, `switch` etc will result in a portion of work-items to do idle work. A general solution does not exist. However some practices like using the trinary operator `?:` if possible etc are better to be followed. Thus the implementation is wholly re-structured to reduce appearance of branch statements. For instance, according to [24], an array of eight strength will be sorted to determine each pedestrian’s next movement at each simulation tick. The sorting was previously accomplished by using the general quick-sort algorithm. Now a tailored algorithm completely based on `?:` is used instead in expense of generality and flexibility.

To map the social field model into the OpenCL heterogeneous framework, factors including those already discussed in the work of [24] are considered so far. Thus it is meaningful to have a summary (table III), among which the issue of competence is more to say. To solve competence without atomic functions, two general methodologies exist. The first one is to interweave operations in a way so that no competition would occur, for example [11]. Unfortunately, such an interweaving may not exist for all of problems including the one being discussed. The second one follows the idea of sacrifice of space in terms of time. However it may cause memory to be exhausted quickly. To solve, the idea of divide-and-conquer can be resorted to set up an upper bound, as what is exhibited in the paper.

5 Numerical Experiments

In order to examine the current GPU model’s numerical efficiency, the scenarios used in the work of [24] are re-experimented. Firstly, the discrete space runs from

$100 \times 100, 200 \times 200, \dots$, to 1000×1000 . Secondly, for each discrete space, the macroscopic density runs from 0.1, 0.2, \dots , to 0.9. Thirdly, all fields' geometry is set to 7×7 . Lastly, for each macroscopic density, the pedestrian flow is assumed to be uni-directional, bi-directional, 4-directional, and 8-directional. This gives total $10 * 9 * 4 = 360$ combinations. Each combination lasts 1000 simulation ticks and repeats 10 times to derive an average running time. Especially, to keep the number of pedestrians constant, the periodic boundary condition is used. And pedestrians' geometry and walk period are all assumed to 1×1 and 1. Figures 8, 9, 10 and 11 give the comparison results.

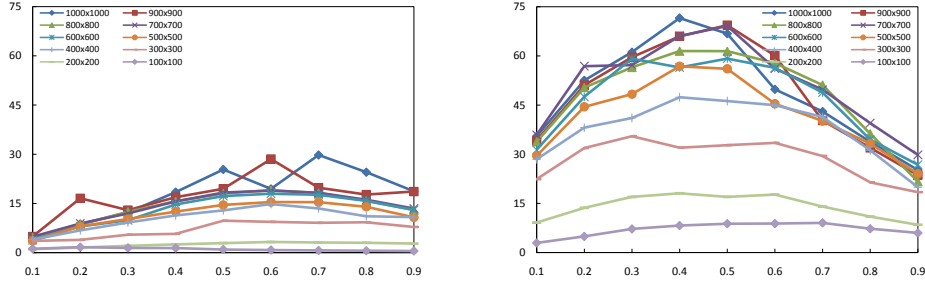


FIG. 8: This exhibits the performance ratios of running times of the CPU model to those of the GPU models for the uni-directional case. The left sub-plot shows the previous GPU model's and the right sub-plot shows the current GPU model's.

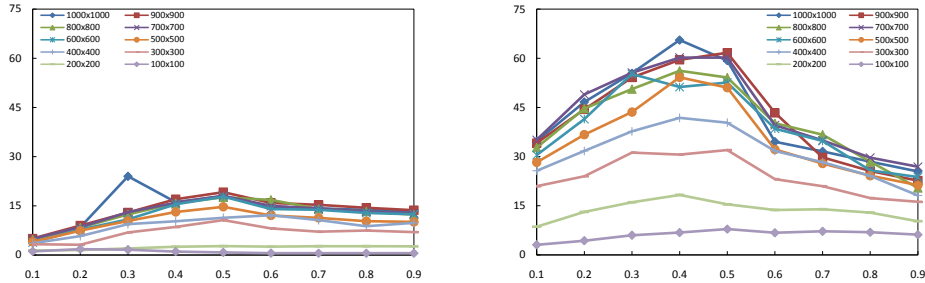


FIG. 9: Performance ratios (bi-directional)

As exhibited, the current GPU model's numerical efficiency is even better. With comparison to the CPU model, the previous GPU model's performance improvement was between 15x and 25x most of the time. And the highest value was 30.8x. Now the current GPU model's performance improvement is between 45x and 60x most of the time, comparing to the CPU model. And the highest value 71.56x happens in the experimented scenario (geometry 700×700 ; density 0.5; 8-directional). This can also be clearly seen in figure 12, which plots all of the 360 performance ratios of running times of the previous GPU model to those of the current GPU model. Furthermore it delineates that the average improvement ratio is 4.44x.

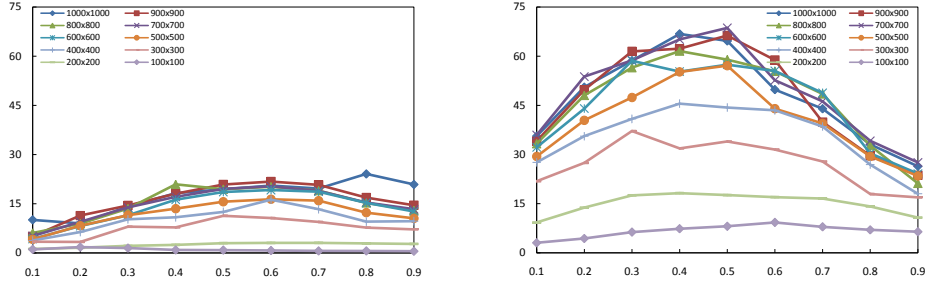


FIG. 10: Performance ratios (4-directional)

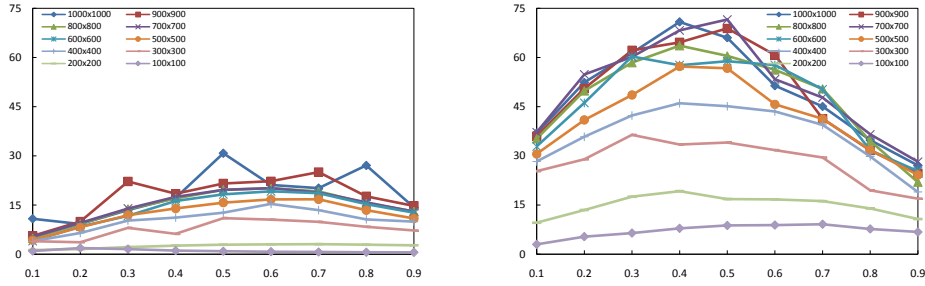


FIG. 11: Performance ratios (8-directional)

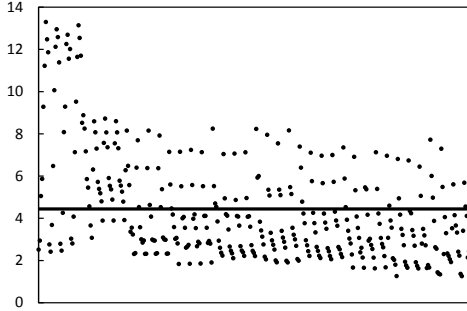


FIG. 12: This exhibits the all 360 performance ratios of running times of the previous GPU model to those of the current GPU model. The maximal performance ratio is 13.3 (geometry 100×100 ; density 0.7; uni-directional). The minimal performance ratio is 1.25 (geometry 1000×1000 ; density 0.9; 4-directional). And the average value is 4.44.

To see the efficiency of the algorithm introduced in the section 3.3, the scenario (geometry 1000×1000 ; density 0.5; 8-directional) is chosen to be the baseline. Then simulations are experimented by letting fields' geometry running from 7×7 , 21×21 , ..., to 77×77 . The examined geometries match the ratios shown in table II. Especially, since pedestrians' geometry is 1×1 and a typical

TABLE IV: Running Times	
geometry	running time (seconds)
7×7	62
21×21	317
35×35	738
49×49	1424
63×63	2187
77×77	3238

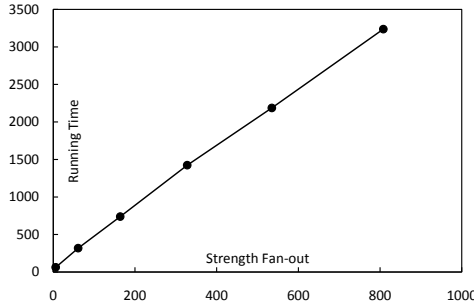


FIG. 13: This exhibits the strict linearity between the running time and strength fan-out.

pedestrian's physical size is $0.3m \times 0.3m$, this is equivalent to consideration of impact of neighboring pedestrians, openings, and obstacles within $0.3m$, $2.1m$, ..., till $23.1m$ in the pedestrian model. The results are given in table IV. In addition, according to algorithm 1, a strict linearity should exist between the running time and strength fan-out, which is exhibited in figure 13.

The concept of walk period was introduced for study of varied walking velocities. The method's most valuable advantage is that no additional complexity will be added to the underlying model logic. In the work of [24], impact of the mechanism upon the numerical efficiency was experimented. With improvements being introduced, the experiments are rerun with the results being given in table V. Except the current GPU model wins again, it is noticed that using a large maximal walk period seems to have different impact on the three models. For example, for the current GPU model, the impact is negligible, but it will cause the previous GPU model to use a long period to finish the simulation.

As aforementioned, in the discrete model, the concept of walk period has an implicit relationship with the space fineness so that pedestrians are allowed to occupy more than one su. A by-product is that the study of jostling is now feasible through dynamically adjusting pedestrians' geometry. Therefore an experiment considering both walk period and dynamic geometry is conducted. Samely the scenario (geometry 1000×1000 ; density 0.5; 8-directional) is used as the baseline. The walk periods run from 1, 3, ..., to 11 and pedestrian

TABLE V: This exhibits running times in second for different walk periods. Again the scenario (geometry 1000×1000 ; density 0.5; 8-directional) is chosen to be the baseline. And simulations are accomplished by keeping the minimal period being 1 and letting the maximal period being 1, 3, ..., and so on. For convenience, it also indicates performance ratios of the current GPU model with comparison to the previous GPU model and the CPU model.

Maximal Period	1	3	5	7	9	11
GPU model (current)	62	64	64	63	62	62
GPU model (previous)	134	203	207	207	208	208
<i>Ratio</i>	<i>2.2</i>	<i>3.3</i>	<i>3.3</i>	<i>3.3</i>	<i>3.4</i>	<i>3.4</i>
CPU model	4114	2478	2581	2436	2452	2456
<i>Ratio</i>	<i>66.4</i>	<i>40.0</i>	<i>41.6</i>	<i>39.3</i>	<i>39.5</i>	<i>39.6</i>

TABLE VI: This exhibits running times for different combinations of walk period and pedestrian geometry. Meanwhile, for each experimented pedestrian geometry, the corresponding number of pedestrians and fields' geometry are also given. For example, for pedestrian geometry 1×1 , the number of pedestrians and fields' geometry are 500000 and 7×7 .

	500000	55555	20000	10204	6172	4132
	7×7	21×21	35×35	49×49	63×63	77×77
	1×1	3×3	5×5	7×7	9×9	11×11
1	63.5	264.6	213.5	207.7	197.6	201.5
3	63.9	261.7	202.0	197.1	186.9	192.5
5	64.0	264.1	204.6	195.5	184.4	191.2
7	63.8	262.9	201.3	193.9	182.0	191.6
9	63.7	262.2	200.1	194.5	184.2	190.5
11	63.9	261.8	200.8	193.8	182.1	189.6

geometries run from 1×1 , 3×3 , ..., to 11×11 . Noteworthy, as the whole space is kept as 1000×1000 , changing pedestrians' geometry will impact the number of pedestrians and fields' geometry. The results are given in table VI. Firstly, it is seen that, for each pedestrian geometry considered, the difference of running times for different walk periods is insignificant. This coincides with the conclusion made in the previous experiment. Secondly, it seems that fields' geometry has a more serious impact. Increasing pedestrians' geometry will both decrease the population and increase fields' geometry in the almost same ratio. But the running time becomes larger with comparing to the basic case where pedestrians' geometry is 1×1 . To some extent, this coincides with the fact that $k=5$ is the most time consuming one among the jobs submitted according to figure 7. Additionally, among the six pedestrian geometries experimented, the one for 3×3 requires the longest running time.

6 Conclusion

In the paper, the previous OpenCL-based implementation of the social field model is improved in two aspects. In one aspect, the problem of memory depletion is solved by the idea of divide-and-conquer. The computational model is now ready to power analysis of super-large scale crowd's complicated and finer walking behaviors. In the other aspect, the OpenCL heterogeneous framework is thoroughly studied and relevant computational techniques are implemented, which brings the numerical efficiency to an even higher level.

With regarding to the future work, first of all the authors plan to develop useful transportation related functional modules, such as XML-based complicated scenario abstraction, macroscopic/mesoscopic route selection algorithms, and so on. Secondly, the authors will set out to study how to use the contemporary information technologies such as deep-learning etc to automatically collect valuable data from raw video images. At the moment, the lack of relevant accurate data is a big problem for quantitative validation and calibration of pedestrian models. The authors believe that the studies together will help scholars to better understand the complex dynamics of evacuation processes.

References

- [1] C. X. Cao, J. Dongarra, P. Du, M. Gates, P. Luszczek, S. Tomov, *clMAGMA: high performance dense linear algebra with OpenCL*, Proceedings of the International Workshop on OpenCL 2013 & 2014
- [2] L. de P. Veronese, R. A. Krohling, *Differential evolution algorithm on the GPU with C-CUDA*, Evolutionary Computation, 2010
- [3] M. Bach, V. Lindenstruth, O. Philipsen, C. Pinke, *Lattice QCD based on OpenCL*, Computer Physics Communications, Volume 184, Issue 9, 2013
- [4] Y. L. Pu, J. Peng, L. T. Huang, *An efficient KNN algorithm implemented on FPGA based heterogeneous computing system using OpenCL*, 23rd Annual International Symposium on Field-Programmable Custom Computing Machines, 2015
- [5] K. Iwai, N. Nishikawa, T. Kurokawa, *Acceleration of AES encryption on CUDA GPU*, International Journal of Networking and Computing, Vol. 2, NO. 1, 2012
- [6] P. Harish and P. J. Narayanan, *Accelerating large graph algorithms on the GPU Using CUDA*, International Conference on High-Performance Computing, 2007
- [7] H. M. Zhu, Y. F. Wu, P. Li, P. Zhang, Z. Ji, M. G. Gong, *An OpenCL-accelerated parallel immunodominance clone selection algorithm for feature selection*, Concurrency and Computation: Practice and Experience, 2016

- [8] M. Garrett, T. Le, V. Nelaturi, L. Shih, *GPU-accelerated cellular automata based finite-difference model for seismic wave propagation with OpenCL*, Proceedings of the Practice and Experience in Advanced Research Computing 2017 on Sustainability, Success and Impact
- [9] N. Khokhlov, A. Ivanov, M. Zhdanov, I. Petrov, E. Ryabinkin, *Applying OpenCL technology for modelling seismic processes using Grid-Characteristic methods*, International Conference on Distributed Computer and Communication Networks, 2016
- [10] M. Molero-Armenta, U. Iturrarán-Viveros, S. Aparicio, M. G. Hernández, *Optimized OpenCL implementation of the elastodynamic finite integration technique for viscoelastic media*, Computer Physics Communications, Vol. 185, Issue 10, 2014
- [11] D. Komatitsch, D. Michéa, G. Erlebacher, *Porting a high-order finite-element earthquake modeling application to NVIDIA graphics cards using CUDA*, Journal of Parallel and Distributed Computing, Vol. 69, Issue 5, 2009
- [12] D. J. Chang, C. Kimmer, M. Ouyang, *Accelerating the Nussinov RNA folding algorithm with CUDA/GPU*, IEEE International Symposium on Signal Processing and Information Technology, 2010
- [13] L. Ligowski, W. Rudnicki, *An efficient implementation of Smith Waterman algorithm on GPU using CUDA, for massively parallel scanning of sequence databases*, Parallel & Distributed Processing, 2009
- [14] G. H. Wang, B. Rister, J. R. Cavallaro, *Workload analysis and efficient OpenCL-based implementation of SIFT algorithm on a smartphone*, 1st Global Conference on Signal and Information Processing, 2013
- [15] G. M. Callicó, S. Lopez, B. Aguilar, J. F. López, R. Sarmiento, *Parallel implementation of the modified vertex component analysis algorithm for hyperspectral unmixing using OpenCL*, IEEE Journal of Selected Topics in Applied Earth Observations and Remote Sensing, Vol. 7, NO. 8, 2014
- [16] B. Keck, H. Hofmann, H. Scherl, M. Kowarschik, J. Hornegger, *GPU-accelerated SART reconstruction using the CUDA programming environment*, Proceedings of SPIE, 2009
- [17] L. Pan, L. X. Gu, J. R. Xu, *Implementation of medical image segmentation in CUDA*, Information Technology and Applications in Biomedicine, 2008
- [18] H. Scherl, B. Keck, M. Kowarschik, J. Jornerger, *Fast GPU-based CT reconstruction using the common unified device architecture (CUDA)*, Nuclear Science Symposium Conference Record, 2007
- [19] J. Wąs, H. Mróz, P. Topa, *GPGPU computing for microscopic simulations of crowd dynamics*, Computing and Information, Vol. 34, 2015

- [20] H. Mróz and J. Wąs, *Discrete vs. continuous approach in crowd dynamics modeling using GPU computing*, Cybernetics and System: An International Journal, 2014
- [21] S. B. Dutta, R. McLeod, M. Friesen, *GPU accelerated nature inspired methods for modelling large scale Bi-directional pedestrian movements*, IEEE International Parallel & Distributed Processing Symposium Workshops, 2014
- [22] A. Rahman, N. A. W. A. Hamid, A. R. Rahiman, *Towards accelerated agent-based crowd simulation for Haji and Umrah*, 2015 International Symposium on Agent, Multi-agent Systems and Robotics
- [23] B. Yu, M. Zhang, Z. R. Wang, *Field based model for pedestrian dynamics*, Journal of Statistical Mechanics: theory and experiment, (2018) 033401
- [24] B. Yu, K. T. Wu, M. Zhang, K. Zhu, Y. H. Ji, *Discretization and OpenCL-based Implementation of Social Field Pedestrian Model*, **under review**